Facile strategy for manipulating micellar size and morphology through intramolecular cross-linking of amphiphilic block copolymers

Ryoto Tanaka, Kodai Watanabe, Takuya Yamamoto, Kenji Tajima, Takuya Isono, Toshifumi Satoh

Graduate School of Chemical Sciences and Engineering, and Division of Applied Chemistry, Faculty of Engineering, Hokkaido University, Sapporo 060-8628, Japan.

Abstract

The effect of intramolecular cross-linking in an amphiphilic block copolymer (BCP) system was systematically investigated in terms of its thermal properties, critical micelle concentration (CMC), and aqueous self-assembly. A series of linear BCPs consisting of poly(ethylene glycol) (PEG) as a hydrophilic block and poly(ε-caprolactone-*co*-7-allyloxepan-2-one) (P(CL-*co*-ACL)) as a hydrophobic block were prepared by the ring-opening copolymerization of ε-caprolactone (CL) and 7-allyloxepan-2-one (ACL) using poly(ethylene glycol) monomethyl ether as the initiator. The intramolecular olefin metathesis reaction in the P(CL-*co*-ACL) block was subsequently carried out under various conditions to prepare the cross-linked BCPs with different degrees of cross-linkings. The thermal analysis confirmed that the linear P(CL-*co*-ACL) block was found to crystallize, while the cross-linked one showed no crystallinity. In addition, the glass transition temperature of the P(CL-*co*-ACL) block increased upon the cross-linking. On the other hand, the intramolecular cross-linking had no significant influence on the CMC. The self-assembled micelles were prepared from the obtained BCPs and their size and morphology investigated. for the BCPs with relatively short PEG chains, the micellar size decreased from 36.6 nm to 16.7 nm as the degree of cross-linking of the P(CL-*co*-ACL) block increased. On the other hand, the BCPs with relatively long PEG chains showed a change in the micellar morphology from spherical micelles to short worm and large compound micelles upon the cross-linking.

Introduction

Amphiphilic block copolymers (BCPs) have attracted increasing interest in recent decades for their ability to self-assemble into ordered nanometric structures in an aqueous medium. The hydrophobic block of the BCP aggregates to form the hydrophobic micelle core, which can play a role as a container and stabilizer for hydrophobic drugs, therefore, the polymeric micelles have been considered to be promising candidates as nanocarriers for therapeutics and biochemicals.[1–5] It is well-known that amphiphilic BCPs produce polymeric micelles with various sizes and morphologies (spherical, cylindrical, vesicular, and lamellar assemblies), and such micellar structural characteristics were found to have a significant impact on the properties and functions as drug delivery nanocarriers. For example, Wang et al. demonstrated that larger polymeric micelles resulted in a higher drug encapsulation efficiency and slower drug release rate.[6] The cross-linking of micellar core was reported to be an interesting approach to produce polymeric micelles with greater stability and better drug loading efficiency.[7,8] In addition, strict control of the micellar size in the range of 10-200 nm is required for avoiding fast excretion through kidney filtration and for targeting tumor cells by the enhanced permeability and retention effect.[9–12] The shape of the micelle also has a critical importance. For example, cylindrical micelles show an increased circulation period and better cell internalization.[13–15] Therefore, the fine-tuning of the BCP self-assembly in terms of size and morphology has been one of the most important issues to be addressed for creating the ideal drug nanocarriers.

A large number of research studies of simple linear BCPs revealed that the molecular weight and hydrophilic/hydrophobic balance are the fundamental parameters for manipulating the size and morphology of the resultant micelles.[16,17] On the other hand, recent improvements in the controlled/living polymerization

systems have largely contributed to the precise design and synthesis of architecturally complex BCPs, such as star, comb, and cyclic BCPs.[18–21] The accessibility to such new types of BCPs enabled systematic studies of the relationship between the BCP architecture and self-assembly behavior. For example, Huh et al. synthesized a series of poly(ethylene glycol)-*b*-poly(ε-caprolactone)s (PEG-*b*-PCL) with simple AB-type linear and AB_2-type miktoarm star-shaped architectures, in which the A and B blocks represent PEG and PCL, respectively, and found that the miktoarm ones self-assembled into cylindrical micelles with a higher drug loading capacity.[22] Moreover, Grayson et al. reported that the macrocyclic BCP formed distinctively smaller micelles as compared to the corresponding linear counterpart.[23] These pioneering studies indicated that the BCP architecture could be a useful factor governing the structure and property of the resultant micelles. It should be emphasized that such a difference in the self-assembly behaviors can be attributed, in part, to the smaller chain dimension of the star or cyclic BCPs as compared to the linear counterparts. Although the macromolecular architecture is highly attractive as the novel fine-tuning strategy of micellar characteristics, such BCPs always suffer from synthetic difficulties.

The intramolecular cross-linking of linear polymers has been gaining increasing attention as a facile method to create a novel type of macromolecular architecture featuring a globular morphology. Generally, intramolecular cross-linking reactions are carried out in sufficiently diluted solution, in which polymer chains rarely collide with each other, thus resulting in the single chain collapse.[24,25] Notably, the intramolecular cross-linking can provide a series of cross-linked polymers having different chain dimensions from the same linear precursor, and the size reduction effect can be obtained much more easily than the star or cyclic polymer synthesis. We Previously established the robust methodology for the precise control of the

polymer chain dimension by the ruthenium-catalyzed olefin metathesis reaction.[26] These facts inspired us to notice that the intramolecular cross-linking can be a novel and efficient mean for the fine-tuning of the BCP self-assembly without changing the molecular weight and hydrophilic/hydrophobic balance. Although a few research groups have demonstrated the intramolecular cross-linking of BCPs,[27–31] the correlation between the degree of the size reduction and the resultant self-assembled nanostructures remains unexplored. In addition, the previous papers focused only on the vinyl polymers, such as the (meth)acrylate- and styrene-based block copolymers, and therefore the application of intramolecular cross-linking to the biocompatible amphiphilic BCPs, just like PEG-*b*-PCL, which is suitable for the biomedical applications, has never been achieved.

Herein, we investigated the effect of the intramolecular cross-linking on the aqueous BCP self-assembly property using the PEG-*b*-PCL system. The BCP consisting of the hydrophilic PEG and the hydrophobic cross-linkable PCL were prepared by the ring-opening copolymerization of ε-caprolactone (CL) and its derivative, *i.e.*, 7-allyloxepan-2-one (ACL), using poly(ethylene glycol) monomethyl ether (mPEG) as the macroinitiator. Subsequently, the poly[(ε-caprolactone)-*co*-(7-allyloxepan-2-one)] (P(CL-*co*-ACL)) block was intramolecularly cross-linked via the olefin metathesis reaction under various conditions to produce the cross-linked BCPs with varied chain dimensions, as shown in Scheme 1. With these BCPs in hand, we investigated the changes in the BCP characteristics, such as the thermal properties, critical micelle concentrations, and aqueous self-assembly behaviors, upon the intramolecular cross-linking by differential scanning calorimetry, fluorescence spectroscopy, and dynamic light scattering/imaging techniques, respectively. Importantly, our results suggest that the intramolecular olefin metathesis can be a

facile strategy for the fine-tuning of the aqueous BCP self-assembly without changing the molecular weight and hydrophilic/hydrophobic balance, leading to a desirable micellar size and morphology.

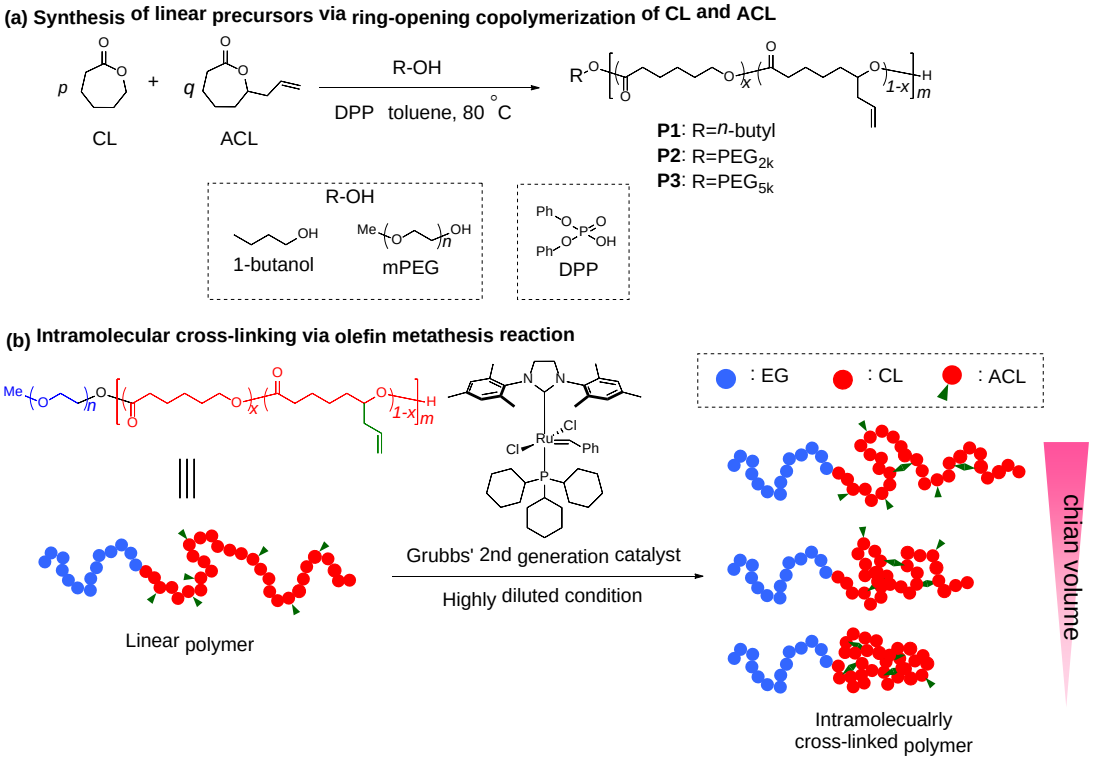

Scheme 1. (a) Diphenyl phosphate (DPP)-catalyzed ring-opening copolymerization of ε-caprolactone (CL) and 7-allyloxepan-2-one (ACL) using 1-butanol or poly(ethylene glycol) monomethyl ether (mPEG) as the initiator. (b) Intramolecular cross-linking via the olefin metathesis reaction to produce a series of intramolecularly cross-linked block copolymers.

Experimental section

Materials. Diphenyl phosphate (DPP; TCI), Amberlyst® A21 (Organo), Grubbs' 2nd generation catalyst (G2; Aldrich), ethyl vinyl ether (TCI), phosphotungstic acid (TAAB laboratories), pyrene (Nakarai tesque), QuadraSil® AP (Wako), and dry tetrahydrofuran (>99.5%; water content <0.001%; Kanto Chemical) were purchased from commercial resources and used as received. 7-Allyloxepan-2-one (ACL) was prepared by following the reported method[32] and purified by distillation over CaH_2 under reduced pressure. ε-Caprolactone (CL; TCI) was purified by distillation over CaH_2 under reduced pressure. 1-Butanol (Kanto Chemical) was purified by distillation over CaH_2 under ambient pressure. Poly(ethylene glycol)monomethyl ethers (mPEGs; Aldrich) with molecular weights of 2000 and 5000 g mol^{-1} were dried by three repeated azeotropic distillations with dry benzene. Dry toluene (Kanto Chemical, >99.5%, water content, <0.001%) was further purified using an MBRAUN solvent purification system (MB SPS COMPACT) equipped with a column of activated alumina and a column of activated copper catalyst. A spectra/Pro® membrane (molecular weight cutoff, 2500) was used for the dialysis.

Instruments. The polymerization was carried out in an MBRAUN stainless steel glovebox equipped with a gas purification system (molecular sieves and a copper catalyst) under a dry argon atmosphere (H_2O, O_2 <0.1 ppm). The ^1H (400 MHz) and ^{13}C NMR (100 MHz) spectra were obtained using a JEOL JNM-ECS400 instrument at 25 °C. Size exclusion chromatography (SEC) was performed at 40 °C in DMF containing lithium chloride (0.01 mol L^{-1}) at the flow rate of 0.6 mL min^{-1} using a JASCO GULLIVER system (JASCO PU-980 pump, JASCO RI-930 reflective index detector, JASCO UV-2075 Plus UV detector, and JASCO DG-2080-53 degasser) equipped with a Shodex KD-G guard column (4.6 mm ×

10 mm; particle size, 8 μm), Shodex GF-7M HQ (linear, 7.5 mm × 300 mm; particle size, 9 μm), and GF-310 HQ columns (linear, 7.5 mm × 300 mm; particle size, 5 μm). A differential scanning calorimetry (DSC) measurement was carried out using a Bruker AXS DSC 3100 differential scanning calorimeter under a N_2 atmosphere in the temperature range from −80 to 100 °C at the heating and cooling rates of 10 °C min^{-1}. The DSC curve was recorded during the first cooling and second heating processes. The mean size of the micelles prepared from the BCPs was determined by dynamic light scattering (DLS) measurements in water using a Beckman Coulter Delsa Nano HC equipped with two semiconductor lasers (wave length, 658 nm; output power, 30 mW; detection angle, 165°; temperature, 25 °C). The emission spectra were recorded by a JASCO FP-6500 spectrofluorometer equipped with a JASCO STR-313 temperature controller (excitation bandwidth = 2.0 nm; emission bandwidth = 2.0 nm; temperature, 15 °C).

Ring-opening copolymerization of CL and ACL. A typical procedure is as follows. In a glovebox, 1-butanol (100 μL, 100 μmol; as 1.0 mol L^{-1} stock solution in dry toluene), CL (528 μL, 5.00 mmol), ACL (360 μL, 2.50 mmol), DPP (25.0 mg, 100 μmol), and dry toluene (6.51 mL) were placed in a Schlenk flask. The flask was sealed with a septum and was taken out from the glovebox. The polymerization was carried out at 80 °C for 22 h, then quenched by adding Amberlyst® A 21. After removing the Amberlyst® A 21, the crude product was purified by dialysis against acetone to give P(CL-*co*-ACL) (**P1**) as a colorless viscous liquid. Yield, 716 mg (74.3%). ^{1}H NMR (400 MHz, $CDCl_3$): δ (ppm), 5.79-5.65 (*m*, −CHCH$_2$C*H*=CH$_2$), 5.11-5.01 (*m*, −CHCH$_2$CH=C*H*$_2$), 4.97-4.86 (*m*, −C*H*CH$_2$CH=CH$_2$), 4.16-3.96 (*m*, −CH$_2$CH$_2$C*H*$_2$O−), 2.39-2.21 (*m*, −OCOC*H*$_2$−), 2.39-2.21 (*m*, −CHC*H*$_2$CH=CH$_2$), 2.19-2.16 (*m*, 2H, CH$_3$CH$_2$CH$_2$−), 1.73-1.51 (*m*, −OCOCH$_2$C*H*$_2$−), 1.73-1.51 (*m*, −OCOCH$_2$CH$_2$CH$_2$C*H*$_2$−), 1.46-1.21 (*m*, −OCOCH$_2$CH$_2$C*H*$_2$−), 0.93 (*t*,

J = 7.5 Hz, 3H, CH_3CH$_2$−). $M_{n,\,SEC}$ = 11600 g mol^{-1}; $M_{n,\,NMR}$ = 9060 g mol^{-1}; $Đ$ = 1.22; the mole fraction of ACL residue (F_{ACL}) = 0.28.

A similar procedure was used for the synthesis of PEG-*b*-P(CL-*co*-ACL)s using mPEG as the initiator instead of 1-butanol. PEG-*b*-P(CL-*co*-ACL) initiated from mPEG$_{2k}$ (**P2**): Yield, 715 mg (82.4%); $M_{n,\,SEC}$ = 14600 g mol^{-1}; $M_{n,\,NMR}$ = 10400 g mol^{-1}; $Đ$ = 1.21; F_{ACL} = 0.28. PEG-*b*-P(CL-*co*-ACL) initiated from mPEG$_{5k}$ (**P3**): Yield, 863 mg (79.0%); $M_{n,\,SEC}$ = 16500 g mol^{-1}; $M_{n,\,NMR}$ = 12400 g mol^{-1}; $Đ$ = 1.24; F_{ACL} = 0.28. ^{1}H NMR (400 MHz, $CDCl_3$): δ (ppm), 5.80-5.66 (*m*, −CHCH$_2$C*H*=CH$_2$), 5.17-5.00 (*m*, −CHCH$_2$CH=C*H*$_2$), 4.96-4.87 (*m*, −C*H*CH$_2$CH=CH$_2$), 4.11-4.00 (*m*, −CH$_2$CH$_2$C*H*$_2$O−), 3.71-3.60 (*m*, −OC*H*$_2$C*H*$_2$O−), 3.38 (*s*, 3H, C*H*$_3$−), 2.38-2.22 (*m*, −OCOC*H*$_2$−), 2.38-2.22 (*m*, −CHC*H*$_2$CH=CH$_2$), 1.72-1.51 (*m*, −OCOCH$_2$C*H*$_2$−), 1.72-1.51 (*m*, −OCOCH$_2$CH$_2$CH$_2$C*H*$_2$−), 1.44-1.23 (*m*, −OCOCH$_2$CH$_2$C*H*$_2$−).

Intramolecular cross-linking of P(CL-*co*-ACL). A typical procedure is as follows. A solution of P(CL-*co*-ACL) (100 mg, 207 μmol-ACL units) in dichloromethane (200 mL) was sonicated for 30 min and degassed by N_2 bubbling. G2 (3.51 mg, 4.14 μmol) was then added to the polymer solution, and the reaction mixture was allowed to be stirred for 5 h at room temperature by gentle N_2 bubbling. After quenching the reaction with an excess amount of ethyl vinyl ether, the solvent was removed under reduced pressure. The residue was dissolved in acetone and treated with QuadraSil® AP to remove the catalyst residue. The mixture was filtered and concentrated to give the cross-linked P(CL-*co*-ACL) as a brown viscous liquid. Yield, 96.5 mg (96.5%). $M_{n,\,SEC}$ = 10600 g mol^{-1}; $M_{n,\,NMR}$ = 8790 g mol^{-1}; $Đ$ = 1.31; the conversion of terminal olefin groups (conv.$_{olefin}$) = 55%. A similar procedure was applied for the intramolecular cross-linking reaction of

P2 and **P3**. The intermolecular cross-linked byproducts could be removed by preparative SEC, if needed. **P2**: Yield, 140 mg (93.2%). $M_{n,SEC}$ = 13000 g mol^{-1}; $M_{n,NMR}$ = 10300 g mol^{-1}; $Đ$ = 1.27; conv.$_{olefin}$ = 69%. **P3**: Yield, 96.4 mg (96.4%). $M_{n,SEC}$ = 15400 g mol^{-1}; $M_{n,NMR}$ = 12700 g mol^{-1}; $Đ$ = 1.29; conv.$_{olefin}$ = 53%.

In case of a reaction in the CH_2Cl_2/*n*-hexane (1/2 v/v) mixed solvent, the reaction mixture was prepared as follows: After sonicating the polymer solution in CH_2Cl_2 for 30 min, *n*-hexane was added dropwise to the mixture with stirring. The final polymer concentration was adjusted to 0.50 g L^{-1}. The resulting solution was further sonicated for 30 min, then the metathesis reaction was started by adding G2.

Preparation of micellar dispersions. The micelle dispersion of the block copolymers was prepared using the nanoprecipitation method.[33] Typically, a block copolymer (2.0 mg) was dissolved in THF (2.0 mL). Subsequently, deionized water (20 mL) was added dropwise to the polymer solution at the rate of 0.1 mL min^{-1} with vigorous stirring. The resulting mixture was subjected to rotary evaporation at room temperature to remove the THF.

Determination of critical micelle concentration (CMC). The CMCs of the PEG-*b*-P(CL-*co*-ACL)s were determined using pyrene as a fluorescent probe as previously reported.[34] A series of micellar dispersions at various concentrations ranging from 0.10 to 3.9×10^{-5} g L^{-1} were prepared by diluting the 0.10 g L^{-1} micellar dispersion that had been prepared according to the above described method. Each micellar dispersion was put into vials containing pyrene and stirred for 24 h prior to the fluorescence measurements. The emission intensity ratio from pyrene at 374 nm and at 384 nm was plotted versus the polymer concentrations, and the CMC was determined from the inflection point of the graph.

Transmittance electron microscopy (TEM). A TEM observation was performed by a JEOL

JEM-2000FX electron microscope operated at the acceleration voltage of 80 kV. The samples for the TEM experiments were prepared by putting one drop of the micelle dispersion onto a copper grid coated with carbon, then dried under atmospheric pressure at room temperature. The sample was negatively stained for 30 s with one drop of a 2 wt % phosphotungstic acid aqueous solution. The excess solution was blotted off using filter paper.

Results and Discussion

Synthesis and characterization. We designed an amphiphilic block copolymer (BCP) consisting of the hydrophilic PEG and the hydrophobic copolymer of CL and ACL (PEG-*b*-P(CL-*co*-ACL)) possessing the cross-linkable olefinic side chain. The targeted BCPs should have well-defined structures and narrow dispersities (*Đ*) in order to elucidate the pure cross-linking effect on the BCP properties. The diphenyl phosphate (DPP)-catalyzed ring-opening polymerization (ROP) of lactones has been known to be a robust and reliable method to produce well-defined aliphatic polyesters with a narrow *Đ*,[35] which let us employ this system for the synthesis of two PEG-*b*-P(CL-*co*-ACL) block copolymers with different PEG chain lengths. The DPP-catalyzed ring-opening copolymerizations of CL and ACL were carried out in toluene at 80 ºC for 22 h at the $[CL]_0/[ACL]_0/[DPP]/[mPEG]_0$ ratio of 50/25/1/1 using mPEGs with the molecular weights of 2000 and 5000 g mol^{-1} to give the PEG-*b*-P(CL-*co*-ACL) amphiphilic BCPs (**P2** and **P3)**, respectively, and the products were isolated in good yield after purification by dialysis against acetone. Figure S2 shows the ^{1}H NMR spectrum of the obtained amphiphilic BCP **P2**. The characteristic signals due to the PEG backbone, P(CL-*co*-ACL) backbone, and methyl protons at the PEG *α*-chain end were observed. The number-average molecular weight ($M_{n,NMR}$) of the P(CL-*co*-ACL) blocks was determined to be 8390 g mol^{-1} for **P2** and 7230 g mol^{-1} for **P3**, and the molar fraction of the ACL residue in the P(CL-*co*-ACL) blocks (F_{ACL}) was calculated to be 0.28 for both products. The SEC trace of the products showed a unimodal molecular weight distribution with the narrow *Đ* of less than 1.24 (Figure 1). Importantly, no mPEG macroinitiator residue was observed in the SEC traces of **P2** and **P3**, confirming the success in the BCP formation without side reactions like the chain transfer reaction. Thus, the targeted amphiphilic BCPs possessing cross-linkable side

chains were successfully obtained. As the model precursor for the following olefin metathesis reaction, the P(CL-*co*-ACL) model copolymer (**P1**) with the $M_{n,NMR}$ of 9060 g mol^{-1}and F_{ACL} of 0.28 was also prepared by the ring-opening copolymerization using 1-butanol as the initiator (Figures S1 and S3).

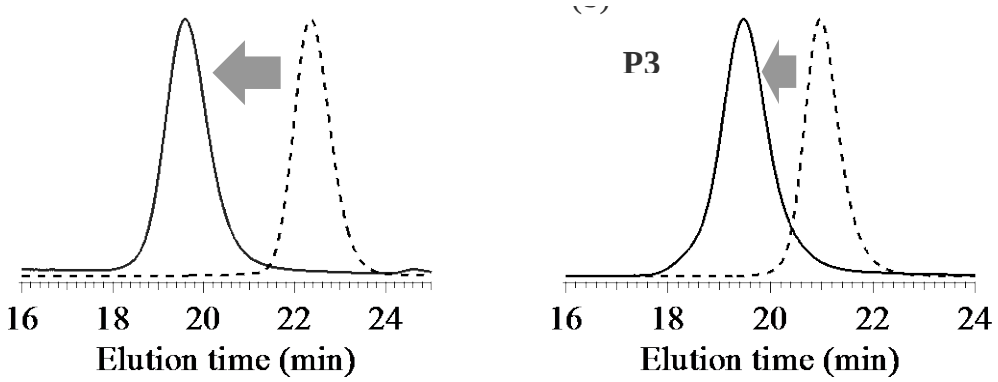

Figure 1. SEC traces of (a) **P2** (solid line) and mPEG$_{2k}$ (dotted line) and (b) **P3** (solid line) and mPEG$_{5k}$ (dotted line). Eluent, DMF containing 0.01 M LiCl; flow rate, 0.6 mL min^{-1}.

Table 1. Ring-opening copolymerization of CL and ACL[a]

polymer	initiator	conv.[b] (%)		F_{ACL}[b,c]	$M_{n,NMR}$[b] (g mol^{-1})		$Đ$[d]	yield
		CL	ACL		PEG	P(CL-*co*-ACL)		(%)
P1	1-butanol	96	75	0.28	-	9060	1.22	74.4
P2	mPEG$_{2k}$	92	71	0.28	2000	8390	1.21	82.4
P3	mPEG$_{5k}$	85	67	0.28	5200	7230	1.24	79.0

[a] Polymerization condition: Ar atmosphere; solvent, toluene; temp., 80 °C; time, 22 h; $[CL]_0/[ACL]_0/[DPP]/[initiator]_0$ = 50/25/1/1; $[CL+ACL]_0$ = 1.0 mol L^{-1}. [b] Determined by ^{1}H NMR in $CDCl_3$. [c] Molar ratio of the ACL residue in the P(CL-*co*-ACL) block. [d] Determined by SEC in DMF containing LiCl (0.01 mol L^{-1}) using polystyrene standards.

Intramolecular cross-linking. According to our previous study, the ruthenium-based olefin metathesis reaction works well even under a highly diluted condition due to the high reactivity of the Grubbs' catalyst. Importantly, the polymer chain dimensions can be controlled by the choice of solvent used for the cross-linking reaction; the polymer chain takes more shrunken conformation in poorer solvent, which results

in better environment to encounter each olefin group, leading to a tightly cross-linked product.[26] We thus carried out the intramolecular olefin metathesis reaction of **P1** under a highly-diluted condition ($[\text{polymer}]_0$ = 0.50 g L^{-1}) in CH_2Cl_2 or a CH_2Cl_2/*n*-hexane (=1/2 (v/v)) mixed solvent in the presence of 2 mol% of Grubbs' 2nd generation catalyst, in which CH_2Cl_2 is a good solvent and *n*-hexane is a poor solvent for the P(CL-*co*-ACL) block (Table 2). The progress of the olefin metathesis reaction was confirmed by the appearance of the new signal due to the internal olefin in the ^{1}H NMR spectra (Figure S4). The conversion of the olefin group ($\text{conv.}_{\text{olefin}}$) in CH_2Cl_2 and CH_2Cl_2/*n*-hexane (=1/2 (v/v)) for 5 h was determined to be 55 and 62%, respectively, and produced soluble products (**P1$_{cl,1}$** and **P1$_{cl,2}$**, respectively). As shown in Figure S7, the SEC traces of the cross-linked products showed a unimodal elution peak in the lower molecular weight region than that of **P1**, which strongly supported the fact that the olefin metathesis reaction successfully proceeded in an intramolecular fashion and the hydrodynamic volume was reduced. In order to discuss the degree of the size reduction of the polymer, we employed a shrinking factor $\langle G \rangle$ defined as the ratio of $M_{n,SEC}$ at the elution peak top ($M_{p,SEC}$) of the cross-linked polymer relative to the linear one, *i.e.*, $\langle G \rangle = M_{p,SEC}(\text{cross-linked})/M_{p,SEC}(\text{linear})$. The $M_{p,SEC}$s of **P1**, **P1$_{cl,1}$**, and **P1$_{cl,2}$** were determined to be 13900, 12600, and 10900 g mol^{-1}, and thus the $\langle G \rangle$ values of **P1$_{cl,1}$** and **P1$_{cl,2}$** were estimated to be 0.91 and 0.78, respectively.

The above-established procedure was applied to the amphiphilic BCP precursors **P2** and **P3**. By tuning the reaction time and/or solvent quality, the cross-linked BCPs with different degrees of size reductions (**P2**$_{cl}$s and **P3**$_{cl}$s) were obtained from **P2** and **P3** (Table 2). Based on the $M_{p,SEC}$ values, the $\langle G \rangle$ value of each cross-linked polymer was calculated to be 0.91 for **P2$_{cl,1}$**, 0.84 for **P2$_{cl,2}$**, and 0.67 for **P2$_{cl,3}$**,

0.89 for **P3$_{cl,1}$**, and 0.86 for **P3$_{cl,2}$** (Figure 2). Here, the $\langle G \rangle$ was defined as ($M_{p,SEC}$(cross-linked) – $M_{p,SEC}$(mPEG))/($M_{p,SEC}$(linear) – $M_{p,SEC}$(mPEG)), in which the $M_{p,SEC}$(mPEG)s were 3120 g mol^{-1} for mPEG$_{2k}$ and 6500 g mol^{-1} for mPEG$_{5k}$. The clean shift in the SEC traces confirmed that the intramolecular cross-linking reactions succeeded even for the BCP.

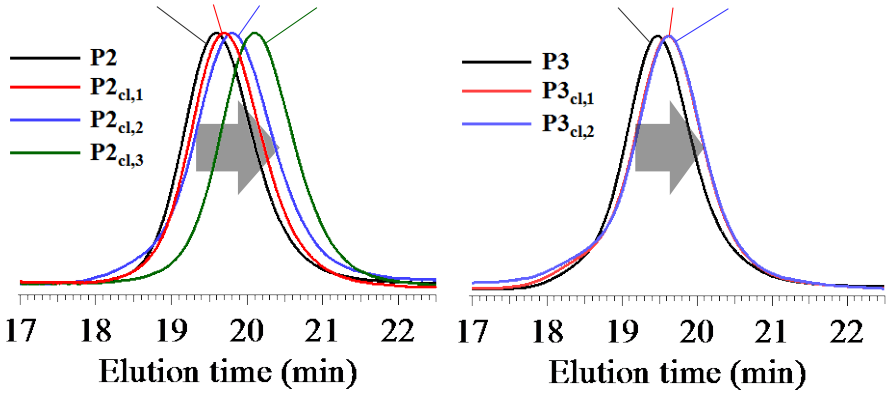

Figure 2. SEC traces of (a) **P2** (black), **P2$_{cl,1}$** (red), **P2$_{cl,2}$** (blue), and **P2$_{cl,3}$** (green) and (b) **P3** (black), **P3$_{cl,1}$** (red), and **P3$_{cl,2}$** (blue). Eluent, DMF containing 0.01 M LiCl; flow rate, 0.6 mL min^{-1}.

Table 2. Intramolecular olefin metathesis reaction [a]

polymer	solvent DCM/*n*-hexane (v/v)	conv.$_{olefin}$ [c] (%)	$M_{n,NMR}$ [c] (g mol^{-1})	$M_{n,SEC}$ [d] (g mol^{-1})	$M_{p,SEC}$ [d,e] (g mol^{-1})	$\langle G \rangle$ [f]	$Đ$ [d]	yield (%)
P1	-	-	9060	11600	13900	1.00	1.22	-
P1$_{cl,1}$	1/0	55	8790	10600	12600	0.91	1.31	96.5
P1$_{cl,2}$	1/2	62	8770	10000	10900	0.78	1.44	84.9
P2	-	-	10400	14600	16400	1.00	1.21	-
P2$_{cl,1}$ [b]	1/0	8.7	10900	13800	14900	0.91	1.19	92.6
P2$_{cl,2}$	1/0	69	10300	13000	13700	0.84	1.27	93.2
P2$_{cl,3}$	1/2	75	10300	10200	10900	0.67	1.19	57.1
P3	-	-	12400	16500	20000	1.00	1.24	-
P3$_{cl,1}$	1/0	53	12700	15400	17900	0.89	1.29	96.4
P3$_{cl,2}$	1/2	51	12700	15300	17200	0.86	1.30	96.3

[a] Reaction conditions: [polymer]$_0$ = 0.50 g L^{-1}; [G2]$_0$/[olefin groups]$_0$ = 0.02; temp., r.t.; reaction time, 5 h. [b] Reaction time, 0.5 h. [c] Determined by ^{1}H NMR in $CDCl_3$. [d] Determined by SEC in DMF containing LiCl

(0.01 mol L^{-1}) using polystyrene standards. [e] $M_{n,SEC}$ at the top of the elusion peak in SEC trace. [f] Calculated from ($M_{p,SEC}$(cross-linked) − $M_{p,SEC}$(mPEG))/($M_{p,SEC}$(linear) − $M_{p,SEC}$(mPEG)), where $M_{p,SEC}$($mPEG_{2k}$) is 0 g mol^{-1} for **P1**, 3120 g mol^{-1} for **P2**, and 6500 g mol^{-1} for **P3**.

Thermal properties. The thermal properties, such as the glass transition temperature (T_g), melting temperature (T_m), and crystallization temperature (T_c) of the obtained polymers were investigated by a DSC analysis. All polymers were first heated to 100 °C and kept for 5 min to erase the thermal history, then cooled to −80 °C, and heated to 100 °C again at the heating and cooling rates of 10 °C min^{-1}. The DSC curves of the linear precursors and the resultant cross-linked products during the second heating process are shown in Figure 3, and the thermal properties of the polymers are listed in Table S1.

In the DSC curves during the second heating process, the linear polymers **P1**-**P3** showed a broad exothermic peak at ca. −23 °C and an endothermic peak at around 3-14 °C, which can be assigned to the crystallization and melting of the P(CL-*co*-ACL) chain, respectively. Meanwhile, such crystallization and melting transitions were not observed in the DSC curves of the cross-linking products, indicating that the cross-linked P(CL-*co*-ACL) chain can no longer crystallize due to the restricted chain conformation. Interestingly, we found that the restricted chain mobility derived from the cross-linking led to an increase in the T_g of the P(CL-*co*-ACL) block, and the more densely the P(CL-*co*-ACL) chain was cross-linked, the higher the T_g value became. For example, **P2** exhibited a T_g at −66.4 °C, while its cross-linked products had the T_g at −63.9 °C for $\mathbf{P2_{cl,1}}$, −57.8 °C for $\mathbf{P2_{cl,2}}$, and −54.0 °C for $\mathbf{P2_{cl,3}}$. On the other hand, no distinctive difference was observed in the T_m of the PEG chain even after the cross-linking reaction.

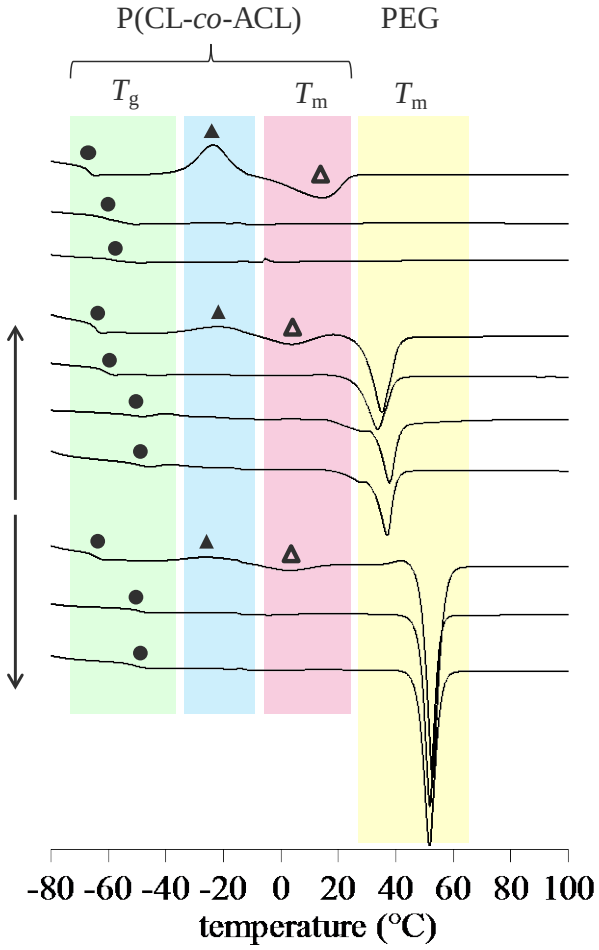

Figure 3. DSC curves during 2nd heating process of (a) **P1**, (b) **P1$_{cl,1}$**, (c) **P1$_{cl,2}$**, (d) **P2**, (e) **P2$_{cl,1}$**, (f) **P2$_{cl,2}$**, (g) **P2$_{cl,3}$**, (h) **P3**, (i) **P3$_{cl,1}$**, and (j) **P3$_{cl,2}$** at the heating rate of 10 °C min^{-1}. The closed circles, the closed triangles, and the open triangles denote the T_g, T_c, and T_m of the P(CL-*co*-ACL) blocks, respectively.

Preparation of micellar dispersion. The aqueous self-assembly of the two series of BCPs was then demonstrated. Because the BCPs synthesized in this study were all insoluble in pure water, we employed the so-called nanoprecipitation method to produce micellar aggregate dispersions in an aqueous medium. This process involves the addition of water to a BCP solution of a water-miscible organic solvent such as THF, DMSO, and DMF, followed by the removal of the organic solvent by either dialysis or evaporation. Generally, the BCP self-assembly based on nanoprecipitation depends on various factors, such as the choice of solvent, method of addition, and method of solvent removal, resulting in various micellar

sizes and morphologies.[33] To exclude the impact of the variations in the preparation method described above, the same nanoprecipitation conditions should be followed to ensure reproducibility. After a thorough screening of the various protocols, we found that the following protocol provides micellar dispersions from a series of BCPs in a reproducible manner: Deionized water (20 mL) was added to a vigorously stirred BCP solution in THF (concentration 1.0 g L^{-1}; 2.0 mL) at the constant rate of 0.1 mL min^{-1}. The corresponding micellar dispersion with the polymer concentration of 0.10 g L^{-1} was then obtained after the THF removal by evaporation.

Effect of intramolecular cross-linking on CMC. As discussed above, the T_gs of the P(CL-*co*-ACL) blocks were much lower than room temperature, and therefore the PEG-*b*-P(CL-*co*-ACL) BCP systems in an aqueous medium should be in thermodynamic equilibrium between the unimer and aggregated state.[36] Amphiphiles in water start aggregating when the polymer concentration reaches a specific value termed the CMC, which is a principal parameter for the thermodynamic stability of the micelle. The CMC values of the micellar dispersions prepared from the obtained BCPs were measured by a fluorescence technique using pyrene as the probe to evaluate the effect of the cross-linking on the micelle stability. It was well-demonstrated that the CMC value is highly affected by the chain length[37–39] and the topology of the hydrophobic block. For example, amphiphilic BCPs having a branched hydrophobic block showed lower CMC values than the corresponding linear BCP.[17,20] On the other hand, the cyclic topology in the hydrophobic block contributed to a rise in the CMC values.[32] The effective chain length and architecture of the hydrophobic block should be changed by the intramolecular cross-linking, thus it can be expected that the cross-linked BCPs show different CMC values from their linear counterparts. Figure S8 shows the plots

of the intensity ratio at the fluorescent wavelengths of 374 nm and 384 nm versus the polymer concentrations on a logarithmic scale. Based on the intersection of the straight lines drawn in Figure S8, the CMC values were calculated to be 0.38 mg L^{-1} for **P2**, 0.45 mg L^{-1} for $\mathbf{P2_{cl,1}}$, 0.44 mg L^{-1} for $\mathbf{P2_{cl,2}}$, 0.41 mg L^{-1} for $\mathbf{P2_{cl,3}}$, 0.76 mg L^{-1} for **P3**, 0.63 mg L^{-1} for $\mathbf{P3_{cl,1}}$, and 0.66 mg L^{-1} for $\mathbf{P3_{cl,2}}$ (Table S1). Contrary to the above expectation, no drastic change in the CMC values among the linear and cross-linked BCPs was observed for both series of **P2** and **P3**, indicating that the intramolecular cross-linking of the hydrophobic block does not affect the thermodynamic stability of the self-assembled structure in an aqueous medium.

Self-assembly of P2 series. **P2** has a short PEG chain relative to the P(CL-*co*-ACL) block, thus **P2** and its cross-linked products should form micellar aggregates surrounded by a thin corona layer of PEG. Such a micelle is known as a “crew-cut” micelle. Figures 4a-d depict the negatively stained TEM images of the micelles prepared from **P2**, $\mathbf{P2_{cl,1}}$, $\mathbf{P2_{cl,2}}$, and $\mathbf{P2_{cl,3}}$, respectively, in which spherical nanoparticles were observed in every case. The number averaged diameter (D_{TEM}) of the micelles was determined to be 24.7 nm for **P2**, 17.2 nm for $\mathbf{P2_{cl,1}}$, 16.4 nm for $\mathbf{P2_{cl,2}}$, and 23.3 nm for $\mathbf{P2_{cl,3}}$. To further investigate the micellar size (hydrodynamic diameter, D_h) and size distribution profile, the DLS measurements were also performed on the micellar dispersions. The number-averaged particle size distributions of the micelles prepared from **P2**, $\mathbf{P2_{cl,1}}$, $\mathbf{P2_{cl,2}}$, and $\mathbf{P2_{cl,3}}$, are shown in Figure 4. These results revealed that each micelle had a unimodal size distribution with a narrow dispersity. In addition, the D_hs of the micelles were determined to be 36.6 nm for **P2**, 26.2 nm for $\mathbf{P2_{cl,1}}$, 16.7 nm for $\mathbf{P2_{cl,2}}$, and 20.1 nm for $\mathbf{P2_{cl,3}}$, indicating that the intramolecularly cross-linked BCPs tended to form smaller micelles than the corresponding linear one, despite their comparable absolute molecular weights and compositions. The linear hydrophobic chains in the micelle core

are stretched to some extent, while the cross-linked ones cannot be stretched due to their restricted chain mobility. Because the degree of stretching of the core-forming block is the dominant factor that determines the diameter of the crew-cut micelle, it should be natural that the decreased hydrophobic chain stretching via the cross-linking directly induced the decrease in the micellar size.[40,41] Indeed, the micellar size tended to decrease with the decreasing ⟨*G*⟩ value. It should be noted that $\mathbf{P2_{cl,3}}$ formed the larger micelle compared to $\mathbf{P2_{cl,2}}$, which disagreed with the tendency described above. We presumed that there is another factor affecting the self-assembly behavior for $\mathbf{P2_{cl,3}}$. When the cross-linking reaction of **P2** was conducted in the mixed solvent with *n*-hexane, entrapment of its own PEG chain inside the cross-linked P(CL-*co*-ACL) block might occur to some extent. Such a PEG-entrapped product in $\mathbf{P2_{cl,3}}$ could behave like a hydrophobic nanoparticle, and this can be incorporated into the micelle core, resulting in the increased micellar size.[30]

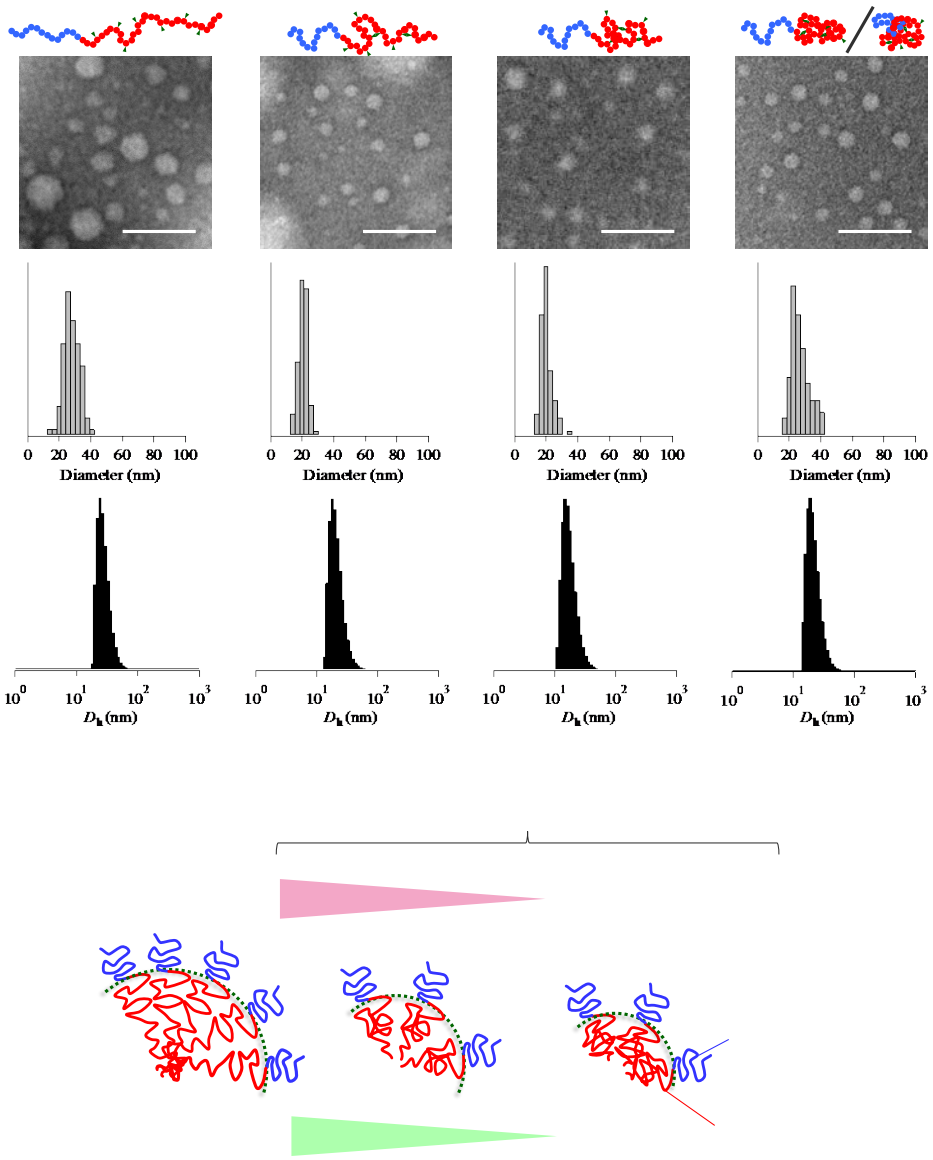

Figure 4. Negatively stained TEM images (top), the number-averaged diameter distributions by TEM (middle), and number-averaged hydrodynamic diameter distributions by DLS (bottom) of the micellar aggregates prepared from (a) **P2**, (b) $\mathbf{P2}_{\mathbf{cl,1}}$, (c) $\mathbf{P2}_{\mathbf{cl,2}}$, and (d) $\mathbf{P2}_{\mathbf{cl,3}}$. Scale bars are 100 nm. (e) Schematic illustration for size transition of micelles prepared from **P2** series.

Self-assembly of P3 series. Contrary to the case of **P2**, **P3** and its cross-linked products should form micellar aggregates possessing a thick corona layer of PEG, and such a micelle is known as a "hairy" micelle. As can be seen in the negatively stained TEM image in Figure 5, the linear BCP, **P3**, formed spherical micelles with the D_{TEM} of 12.2 nm. The DLS plot also indicated a unimodal particle size distribution with the D_h of 13.0 nm. It should be mentioned that **P3** formed a smaller micelle than **P2** in spite

of the longer PEG chain, which should be attributed to the higher interfacial curvature.[16,42] On the other hand, the DLS plots for the micellar dispersions prepared from the cross-linked BCPs, **P3$_{cl,1}$** and **P3$_{cl,2}$**, displayed bimodal size distributions. The D_h values for the major and minor populations were 16.3 and 69.5 nm for **P3$_{cl,1}$** and 21.8 and 92.8 nm for **P3$_{cl,2}$**, respectively, and these values increased as the $\langle G \rangle$ value of the BCP decreased. In the TEM images of **P3$_{cl,1}$**, the short worm-like micelles were observed along with the major component of the spherical micelles. Likewise, the coexistence of distinctively large spherical aggregates likely due to a large compound micelle (LCM) was observed in the TEM images of **P3$_{cl,2}$** along with the major component of spherical micelles. Therefore, the larger species in the DLS plots should be assigned to the worm-like micelle for **P3$_{cl,1}$** and the LCM for **P3$_{cl,2}$**. The linear BCPs seem to take a cone-like molecular shape in the micelle because of the strong repulsion between the corona chains so that the resultant micelle was forced to be spherical with a high curvature (Figure 5d). On the other hand, the globular conformation of the cross-linked P(CL-*co*-ACL) block causes a local crowding on the hydrophobic side of the core-shell interface, resulting in the change in the molecular shape from cone-like to cylinder-like and a decrease in the interfacial curvature. Such a transformation of the entire molecular shape resulted in the morphological transition from a spherical micelle into the micellar aggregate with lower curvatures such as the short worm-like micelle and LCM.

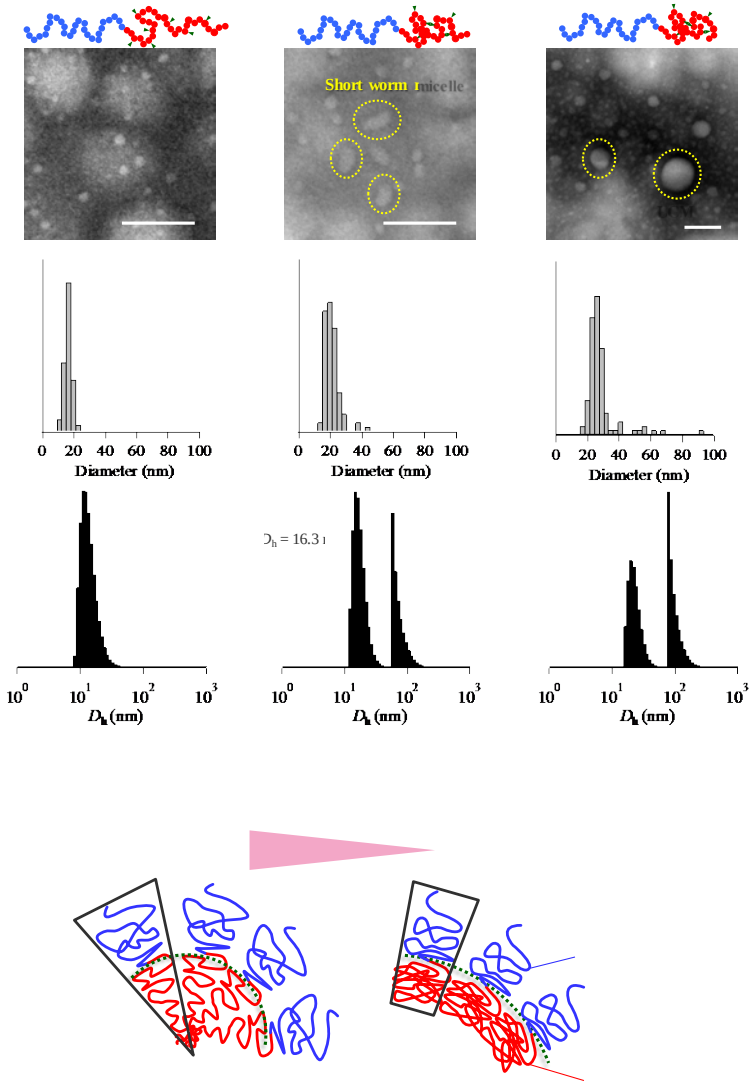

Figure 5. Negatively stained TEM images (top), the number-averaged diameter distributions by TEM (middle), and number-averaged hydrodynamic diameter distributions by DLS (bottom) of the micellar aggregates prepared from (a) **P3**, (b) $\mathbf{P3_{cl,1}}$, and (c) $\mathbf{P3_{cl,2}}$. Scale bars are 100 nm. (d) Schematic illustration of morphology transition prepared from **P3** series.

Conclusions.

The thermal properties, CMC, and self-assembly behaviors of the intramolecularly cross-linked PEG-*b*-P(CL-*co*-ACL)s were evaluated in order to investigate the intramolecular cross-linking effects in the amphiphilic BCP system. The DSC analysis revealed that the intramolecular cross-linking suppressed the molecular mobility and crystallization of the P(CL-*co*-ACL) block, which caused the absence of crystallinity and increase in the T_g value. In contrast to the thermal behaviors, no significant difference was observed in the CMC values among the linear and cross-linked BCPs, indicating that the intramolecular cross-linking hardly affects the hydrophilicity of the BCP as well as the thermodynamic stability of the resulting micelles. As we expected, the PEG-*b*-P(CL-*co*-ACL)s and the cross-linked products successfully self-assembled into micellar aggregates in water. A thorough analysis of the micellar aggregates by DLS and TEM measurements revealed that the intramolecular cross-linking of the core-forming block largely affected the self-assembling behaviors. In the case of **P2** and its cross-linked BCPs, the micellar size decreased with the decreasing $\langle G \rangle$ value due to the restricted chain stretching of the core-forming block. In the case of **P3** and its cross-linked BCPs, on the other hand, the cross-linking of the core-forming block led to a change in the micellar morphology. Our results demonstrated that the intramolecular olefin metathesis of amphiphilic BCPs can be a robust and facile methodology for the fine-tuning of the micellar size and morphology without changing the molecular weight and composition, which will be helpful in fabricating nanocarriers or nanocontainers, with specific structures and functions, for a range of applications.

Acknowledgements

This work was financially supported by the MEXT Grant-in-Aid for Research Activity Start-up (26888001) and Grant-in-Aid for Young Scientists (B) (15K17862).

Notes and References

1 E. K. Park, S. Y. Kim, S. B. Lee and Y. M. Lee, *J. Control. Release*, 2005, **109**, 158–168.

2 C. Allen, J. Han, Y. Yu, D. Maysinger and A. Eisenberg, *J. Control. Release*, 2000, **63**, 275–286.

3 T. Riley, S. Stolnik, C. R. Heald, C. D. Xiong, M. C. Garnett, L. Illum, S. S. Davis, S. C. Purkiss, R. J. Barlow and P. R. Gellert, *Langmuir*, 2001, **17**, 3168–3174.

4 M. Danquah, T. Fujiwara and R. I. Mahato, *J. Polym. Sci. Part A Polym. Chem.*, 2013, **51**, 347–362.

5 K. Kataoka, A. Harada and Y. Nagasaki, *Adv. Drug Deliv. Rev.*, 2001, **47**, 113–131.

6 Y. Hu, J. Xie, Y. W. Tong and C.-H. Wang, *J. Control. Release*, 2007, **118**, 7–17.

7 M. Iijima, Y. Nagasaki, T. Okada, M. Kato and K. Kataoka, *Macromolecules*, 1999, **32**, 1140–1146.

8 X. Shuai, T. Merdan, A. K. Schaper, F. Xi and T. Kissel, *Bioconjug. Chem.*, 2004, **15**, 441–448.

9 H. Soo Choi, W. Liu, P. Misra, E. Tanaka, J. P. Zimmer, B. Itty Ipe, M. G. Bawendi and J. V Frangioni, *Nat. Biotechnol.*, 2007, **25**, 1165–1170.

10 X.-B. Xiong, A. Falamarzian, S. M. Garg and A. Lavasanifar, *J. Control. Release*, 2011, **155**, 248–261.

11 J. Fang, H. Nakamura and H. Maeda, *Adv. Drug Deliv. Rev.*, 2011, **63**, 136–151.

12 T. Sun, Y. S. Zhang, B. Pang, D. C. Hyun, M. Yang and Y. Xia, *Angew. Chemie - Int. Ed.*, 2014, **53**, 12320–12364.

13 S. Matsumura, A. R. Hlil, C. Lepiller, J. Gaudet, D. Guay, Z. Shi, S. Holdcroft and A. S. Hay, *Am. Chem. Soc. Polym. Prepr. Div. Polym. Chem.*, 2008, **49**, 511–512.

14 K. Zhang, H. Fang, Z. Chen, J.-S. A. Taylor and K. L. Wooley, *Bioconjug. Chem.*, 2008, **19**, 1880–1887.

15 Y. Geng, P. Dalhaimer, S. Cai, R. Tsai, M. Tewari, T. Minko and D. E. Discher, *Nat. Nanotechnol.*, 2007, **2**, 249–255.

16 L. Zhang and A. Eisenberg, *J. Am. Chem. Soc.*, 1996, **118**, 3168–3181.

17 A. Blanazs, S. P. Armes and A. J. Ryan, *Macromol. Rapid Commun.*, 2009, **30**, 267–277.

18 G. M. Soliman, R. Sharma, A. O. Choi, S. K. Varshney, F. M. Winnik, A. K. Kakkar and D. Maysinger, *Biomaterials*, 2010, **31**, 8382–8392.

19 J. Yun, R. Faust, L. S. Szilágyi, S. Kéki and M. Zsuga, *Macromolecules*, 2003, **36**, 1717–1723.

20 S. Sinnwell, A. J. Inglis, M. H. Stenzel and C. Barner-Kowollik, *Macromol. Rapid Commun.*, 2008, **29**, 1090–1096.

21 J. H. Zhongyu Li, Pengpeng Li, *J. Polym. Sci. Part A Polym. Chem.*, 2006, **44**, 4361–4371.

22 K. Yoon, H. C. Kang, L. Li, H. Cho, M.-K. Park, E. Lee, Y. H. Bae and K. M. Huh, *Polym. Chem.*, 2015, **6**, 531–542.

23 B. Zhang, H. Zhang, Y. Li, J. N. Hoskins and S. M. Grayson, *ACS Macro Lett.*, 2013, **2**, 845–848.

24 M. K. Aiertza, I. Odriozola, G. Cabañero, H.-J. Grande and I. Loinaz, *Cell. Mol. Life Sci.*, 2012, **69**, 337–346.

25 S. Mavila, O. Eivgi, I. Berkovich and N. G. Lemcoff, *Chem. Rev.*, 2016, **116**, 878–961.

26 K. Watanabe, R. Tanaka, K. Takada, M.-J. Kim, J.-S. Lee, K. Tajima, T. Isono and T. Satoh, *Polym. Chem.*, 2016, **7**, 4782–4792.

27 E. Harth, B. Van Horn, V. Y. Lee, D. S. Germack, C. P. Gonzales, R. D. Miller and C. J. Hawker, *J. Am. Chem. Soc.*, 2002, **124**, 8653–8660.

28 J. Wen, L. Yuan, Y. Yang, L. Liu and H. Zhao, *ACS Macro Lett.*, 2013, **2**, 100–106.

29 W. Li, S. Thanneeru, I. Kanyo, B. Liu and J. He, *ACS Macro Lett.*, 2015, **4**, 736–740.

30 Y. Kim, J. Pyun, J. M. J. Fréchet, C. J. Hawker and C. W. Frank, *Langmuir*, 2005, **21**, 10444–10458.

31 W. Li, C.-H. Kuo, I. Kanyo, S. Thanneeru and J. He, *Macromolecules*, 2014, **47**, 5932–5941.

32 G. Dyker and P. Grundt, *European J. Org. Chem.*, 1999, **1999**, 323–327.

33 U. Bilati, E. Allémann and E. Doelker, *Eur. J. Pharm. Sci.*, 2005, **24**, 67–75.

34 T. Isono, Y. Satoh, K. Miyachi, Y. Chen, S. Sato, K. Tajima, T. Satoh and T. Kakuchi, *Macromolecules*, 2014, **47**, 2853–2863.

35 K. Makiguchi, T. Satoh and T. Kakuchi, *Macromolecules*, 2011, **44**, 1999–2005.

36 K. Letchford and H. Burt, *Eur. J. Pharm. Biopharm.*, 2007, **65**, 259–269.

37 I. Astafieva, X. F. Zhong and A. Eisenberg ', *Macromolecules*, 1993, **26**, 7339–7352.

38 C. Allen, D. Maysinger and A. Eisenberg, *Colloids Surfaces B Biointerfaces*, 1999, **16**, 3–27.

39 I. Gyun Shin, S. Yeon Kim, Y. Moo Lee, C. Soo Cho and Yong Kiel Sung, *J. Control. Release*, 1998, **51**, 1–11.

40 T. Isono, K. Miyachi, Y. Satoh, R. Nakamura, Y. Zhang, I. Otsuka, K. Tajima, T. Kakuchi, R. Borsali and T. Satoh, *Macromolecules*, 2016, **49**, 4178–4194.

41 L. Zhang and A. Eisenberg, *Macromolecules*, 1999, **32**, 2239–2249.

42 L. Zhang, R. J. Barlow and A. Eisenberg, *Macromolecules*, 1995, **28**, 6055–6066.

Table of Contents

Facile strategy for manipulating micellar size and morphology through intramolecular cross-linking of amphiphilic block copolymers

Ryoto Tanaka, Kodai Watanabe, Takuya Yamamoto, Kenji Tajima, Takuya Isono, Toshifumi Satoh

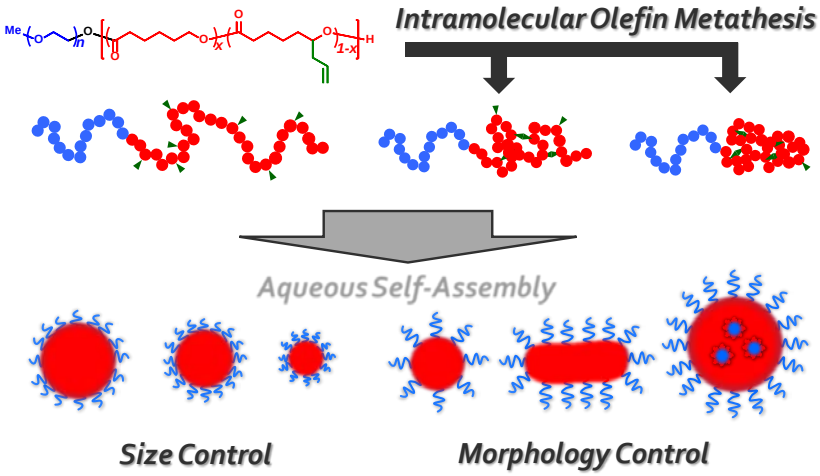

Effect of intramolecular cross-linking on aqueous self-assembly behavior was systematically investigated based on the amphiphilic block copolymer system.